Photochemical modelling of atmospheric oxygen levels confirms two stable states

Bethan S. Gregory [a,b,*], Mark W. Claire [a,b,c], Sarah Rugheimer [d]

[a] School of Earth and Environmental Sciences, University of St Andrews, St Andrews, KY16 9AL, UK
[b] Centre for Exoplanet Sciences, University of St Andrews, St Andrews, KY16 9AL, UK
[c] Blue Marble Space Institute of Science, 1001 4th Ave, Suite 3201, Seattle, WA 98154, USA
[d] Department of Physics, University of Oxford, Oxford, OX1 3PU, UK

ABSTRACT

Various proxies and numerical models have been used to constrain O_2 levels over geological time, but considerable uncertainty remains. Previous investigations using 1-D photochemical models have predicted how O_3 concentrations vary with assumed ground-level O_2 concentrations, and indicate how the ozone layer might have developed over Earth history. These classic models have utilised the numerical simplification of fixed mixing ratio boundary conditions. Critically, this modelling assumption requires verification that predicted fluxes of biogenic and volcanic gases are realistic, but also that the resulting steady states are in fact stable equilibrium solutions against trivial changes in flux.

Here, we use a 1-D photochemical model with fixed flux boundary conditions to simulate the effects on O_3 and O_2 concentrations as O_2 (and CH_4) fluxes are systematically varied. Our results suggest that stable equilibrium solutions exist for trace- and high-O_2/O_3 cases, separated by a region of instability. In particular, the model produces few stable solutions with ground O_2 mixing ratios between 6×10^{-7} and 2×10^{-3} (3×10^{-6} and 1% of present atmospheric levels). A fully UV-shielding ozone layer only exists in the high-O_2 states. Our atmospheric modelling supports prior work suggesting a rapid bimodal transition between reducing and oxidising conditions and proposes Proterozoic oxygen levels higher than some recent proxies suggest. We show that the boundary conditions of photochemical models matter, and should be chosen and explained with care.

1. Introduction

Improved constraints of atmospheric oxygen levels over Earth history are important for an enriched understanding of how life and Earth have co-evolved. Molecular oxygen (O_2) currently makes up 21% of the atmosphere, but this has not always been the case. The disappearance of sulphur isotope mass-independent fractionation (S-MIF) in the geological record at 2.4-2.5 Ga (Bekker et al., 2004; Farquhar et al., 2000; Warke et al., 2020) is considered strong evidence for the Great Oxidation Event (GOE). To explain this, models require the partial pressure of oxygen (pO_2, also referred to as the O_2 mixing ratio) to be less than 2.1×10^{-6} (10^{-5} times the present atmospheric level (PAL)) for the Archaean and more than 2.1×10^{-6} after the GOE (Pavlov and Kasting, 2002).

However, uncertainty remains regarding atmospheric O_2 levels since the GOE (see e.g. reviews by Farquhar et al. (2014); Kump (2008); Lyons et al. (2014)), in particular for the Proterozoic, where palaeo-O_2 proxies yield differing constraints. Proxies for Proterozoic oxidative weathering and ocean oxygenation have classically led to pO_2 estimates between 2.1×10^{-3} and 0.084 (Canfield, 1998, 2005; Holland, 1994; Johnson et al., 2014; Lenton and Daines, 2017; Rye and Holland, 1998). The existence of an ozone layer, indicated by the presence of mass-independently fractionated oxygen isotopes (O-MIF) in sedimentary sulphates since the GOE (Crockford et al., 2019), is thought to require pO_2 exceeding 2.1×10^{-4} (Segura et al., 2003), while model interpretations of large, negative O-MIF from 1.4 Ga sulphates (Crockford et al., 2018) suggest an upper limit of 2.1×10^{-3} for this period (Planavsky et al., 2020). This upper limit is consistent with cerium anomalies from 1.87 Ga (Bellefroid et al., 2018) and a lack of fractionation of sedimentary chromium isotopes, interpreted to indicate pO_2 lower than 2.1×10^{-3} or even 2.1×10^{-4} for parts of the Proterozoic before 0.8 Ga (Cole et al., 2016; Planavsky et al., 2014, 2018). However, the timing of the appearance of variable $\delta^{53}Cr$

(and its interpretation) in the geological record is debated, with some studies predicting much higher pO_2 between 0.8 and 1.1 Ga (Gilleaudeau et al., 2016) and even further back in the Mesoproterozoic (Canfield et al., 2018). Even for the Phanerozoic, where the continuous presence of animal life indicates relatively high oxygen levels, uncertainty remains (Krause et al., 2018). For the last 400 Myr, a continuous charcoal record suggests oxygen levels between 15% and 30% (Bergman et al., 2004; Glasspool and Scott, 2010; Glasspool et al., 2015).

Previous 1-D photochemical models (Kasting and Donahue, 1980; Kasting et al., 1985; Segura et al., 2003; Zahnle et al., 2006) have investigated potential palaeo-atmospheres by explicitly constructing models with a range of pO_2. These models utilised 'fixed mixing ratio' lower boundary conditions (LBCs) for O_2, in which the experimenter sets the pO_2 and the model is allowed to vary fluxes across the lower boundary and other species' concentrations to produce a steady-state solution which satisfies the given boundary conditions. In a brief summary overview, these previous studies (reproduced below) found that the ozone column density (the number of ozone molecules in an atmospheric column with a surface area of one square centimetre) initially increases as a power-law with pO_2, before saturating at higher O_2 concentrations (Fig. 1a).

The results of these 1-D photochemical modelling studies have been simplified, parametrised and incorporated into a number of Earth system evolution models, which include shorter-term biological and atmospheric feedbacks with longer-term planetary redox fluxes, such as volcanic degassing and hydrogen escape. Intriguingly, these models have predicted bimodal behaviour with respect to oxygen concentrations. For example, the 2-box model of Goldblatt et al. (2006) predicted two regions only: $pO_2 < 2.1 \times 10^{-6}$ and $pO_2 > 10^{-3}$. Similarly, the 3-box biogeochemical model of Laakso and Schrag (2017) found stable solutions with $pO_2 < 2.1 \times 10^{-8}$ and $pO_2 > 2.1 \times 10^{-4}$. Other biogeochemical models predict a 'GOE' in which O_2 mixing ratios change from 10^{-6} to 2×10^{-3} (Claire et al., 2006) or 10^{-2} (Alcott et al., 2019) relatively quickly. While biological re-organisation to oxic conditions provides a positive feedback (Catling et al., 2007; Daines and Lenton, 2016), the primary driver captured is the development of an ozone layer which shields O_2 from photolysis (Claire et al., 2006; Goldblatt et al., 2006), as captured by parametrisations of 1-D photochemical models.

Here, we revise the classic photochemical modelling calculations which relate O_2 and O_3, by utilising 'fixed flux' LBCs for O_2 and other gases. The O_2 flux into the atmosphere is specified by the experimenter, and the model predicts the resulting mixing ratio profiles in equilibrium with the radiation field, kinetics, and other physical processes (e.g. lightning, particle formation, condensation). Flux boundary conditions represent a closer conceptual match to what real atmospheres do (e.g. fluxes vary and concentrations adjust), compared to the assumption that the planetary and biogenic fluxes somehow adjust in order to maintain fixed ground-level concentrations. First, we briefly introduce the 1-D photochemical model, *Atmos*. In Section 3, we use *Atmos* with fixed mixing ratio LBCs for O_2 to replicate previous results, but observe that these models predict potentially unrealistic fluxes. Our primary results comprise a systematic study of atmospheric chemistry resulting from variable O_2 and methane fluxes across the lower boundary. Specifically, we i) vary O_2 fluxes at several fixed CH_4:O_2 flux ratios (Section 4.1); ii) vary CH_4:O_2 flux ratios at several fixed O_2 fluxes (Section 4.2); and explore sensitivity to iii) oxidative weathering (Section 4.4) and iv) other important redox fluxes (Section 4.6).

Our investigation of 2067 flux-driven model atmospheres reveals a bimodal oxygen distribution similar to those observed in biogeochemical models, but one that arises entirely in the atmo-
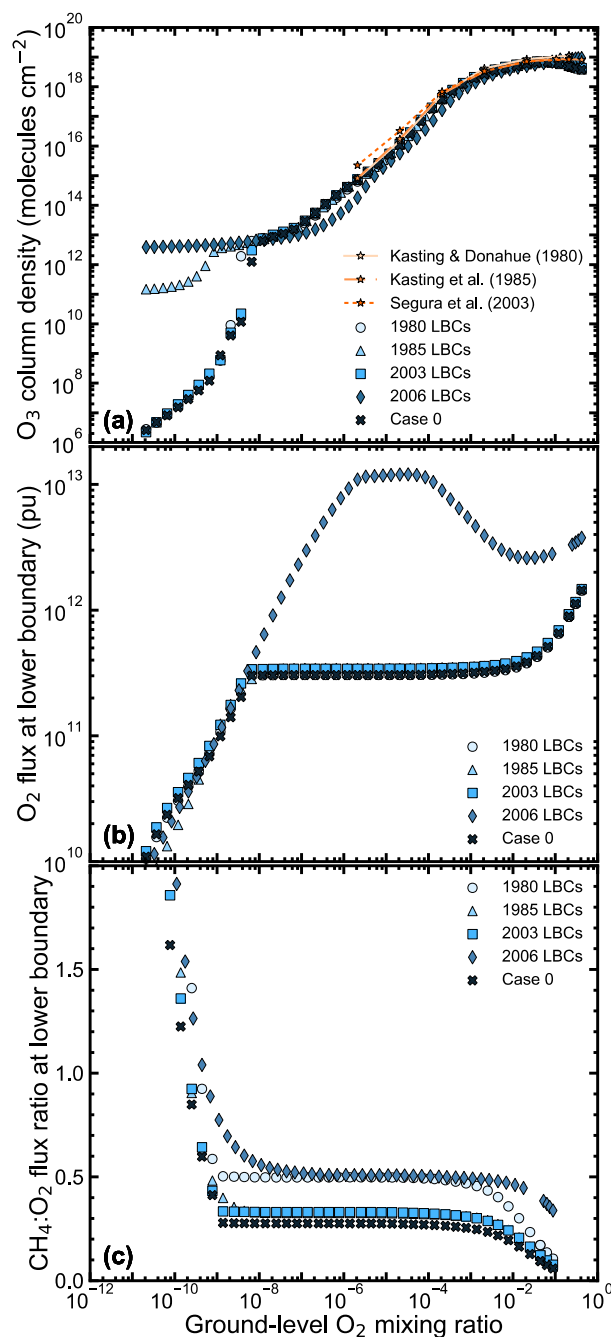
Fig. 1. Extracted model results from suites using fixed mixing ratio lower boundary conditions for O_2.

Circles, triangles, squares and diamonds show results using *Atmos* with the same boundary conditions as previous authors. '1980 LBCs,' '1985 LBCs,' '2003 LBCs' and '2006 LBCs' refer to the boundary conditions used by Kasting and Donahue (1980), Kasting et al. (1985), Segura et al. (2003) and Zahnle et al. (2006), respectively. Crosses show Case 0 results, with fixed mixing ratio boundary conditions for O_2 and fixed flux boundary conditions for CH_4, H_2, CO and N_2O. For the boundary conditions used, see Table 1. **(a)** Ozone column densities with user-specified ground-level O_2 mixing ratio. The results from previous studies are also shown (orange lines). **(b)** Predicted oxygen fluxes, and **(c)** predicted CH_4:O_2 flux ratios required to produce the fixed mixing ratio model atmospheres, plotted against user-specified O_2 mixing ratio. (For interpretation of the colours in the figures, the reader is referred to the web version of this article.)

sphere itself. We explicitly demonstrate that some classic results are unstable equilibrium solutions (Section 4.3) and argue that many intermediate oxygen concentrations are photochemically unstable. In Section 5, we discuss implications for palaeo-O_2 con-

straints, provide suggestions for future work in both photochemical and biogeochemical modelling, and argue that the choice of numerical methods used by 1-D photochemical models has implications for how the Earth system science community considers the evolution of atmospheric oxygen.

2. Model description

We use the one-dimensional photochemical model *Atmos* (open source code available via https://github.com/VirtualPlanetaryLaboratory/atmos), most recently described in Arney et al. (2016). The 'ModernEarth+Cl' template utilised in this study incorporates 87 atmospheric species involved in 372 reactions, whose rates have been updated to follow recent recommendations (Table D1). An altitude grid of 160 0.5 km layers gives a simulated atmosphere of height 80 km, with the tropopause set at 11 km, suitable for a mid-latitude profile. Each model presented here was run with modern eddy diffusion and temperature profiles (Appendix E), and we analyse only steady-state solutions. The lower boundary of the model represents Earth's surface, across which we prescribe fluxes of volcanic and biogenic gases into the bottom-most model grid layer, in addition to gaseous, aqueous and particulate deposition out of the model atmosphere. LBCs are specified for each atmospheric species (Tables B1 and C1) and discussed further below.

3. Results from fixed mixing ratio photochemical modelling

We used fixed mixing ratio LBCs for O_2 to compare outputs from *Atmos* to the results of previous studies (shown in Fig. 1a). Kasting and Donahue (1980), Kasting et al. (1985) and Segura et al. (2003) used fixed flux or deposition velocity (specifying the removal rate from the atmosphere) LBCs for CH_4, H_2, CO and N_2O. The magnitudes of these fluxes were determined by predicted fluxes from a fixed mixing ratio LBC model simulating the modern Earth for these species (with the exception of Kasting and Donahue's (1980) H_2 and CO, which were allocated zero flux LBCs). Resulting negative (i.e. out of the atmosphere into the ocean) H_2 fluxes led Kasting et al. (1985) and Segura et al. (2003) to use deposition velocity and negative fixed flux boundary conditions for H_2, respectively. Zahnle et al. (2006) used fixed mixing ratio LBCs for CH_4, and chose large positive fluxes of H_2 and CO. These (and all LBCs used in this study) are summarised in Table 1. We specify units of flux in 'photochemical units' or 'pu' (1 pu = 1 molecule cm^{-2} s^{-1} ∼ 2.7×10^{-10} Tmol yr^{-1}).

Using *Atmos*, we produced suites of steady-state model atmospheres with O_2 ground-level mixing ratios varying between 2.1×10^{-11} and 0.42, choosing LBCs using the specific methods of the previous four studies. A fifth suite (hereafter referred to as Case 0; see Table 1) also incorporates fixed flux LBCs for CH_4, CO and N_2O equal to those computed by modern fixed mixing ratio calculations. Like the models of Kasting et al. (1985) and Segura et al. (2003), *Atmos* predicts a net flux of H_2 out of the atmosphere when run solely with modern fixed mixing ratio LBCs. This is physically unrealistic and numerically allows models significant leeway to mask redox imbalances by dumping hydrogen into the (assumed) ocean. We incorporated the predicted fluxes as fixed flux LBCs and tuned them, primarily by slightly reducing the larger (biogenic) CH_4 flux, to achieve an atmosphere predicting modern mixing ratios for the five species, but with a net flux of H_2 into the atmosphere within an order of magnitude of the modern volcanic flux (Aiuppa et al., 2011). A fixed mixing ratio LBC for preindustrial CO_2 (280 ppmv) was used. Allowing the model to compute CO_2 fluxes is justifiable here as CO_2 is redox-neutral, whereas O_2, CH_4, H_2, CO and N_2O are not (Zahnle et al., 2006).

The ozone column density increases with specified ground-level pO_2 but plateaus above a pO_2 of 10^{-2}, following a chemical pattern discussed in previous work (Fig. 1a). Differences between our models for trace-O_2 concentrations are primarily due to the different choices of boundary conditions. Our results are very similar to those of previous models, with small changes due to updated kinetic rate coefficients, which is unsurprising given that *Atmos* shares a common code heritage. However, in what follows we discuss observations that led us to discover that some of the steady-state model atmospheres predicted by fixed mixing ratio LBCs exhibit behaviour of unstable equilibrium solutions.

3.1. The restrictions of a fixed mixing ratio boundary condition

By construction, fixed mixing ratio LBCs enable the model to vary lower boundary fluxes to produce the user-specified concentration, but the required fluxes may not be physically realistic. Fig. 1b shows the O_2 fluxes computed by the model to maintain the specified O_2 mixing ratio boundary conditions in Fig. 1a. These fluxes (and others not shown) vary across the experiments, making the direct comparison of simulated atmospheres challenging, and are not necessarily representative of how a real biosphere would function. For example, Fig. 1c shows that though the predicted CH_4:O_2 flux ratio is ∼0.1 for most high-O_2 atmospheres, consistent with theoretical estimates and modern measurements, the CH_4:O_2 flux ratio varies significantly for moderate-O_2 atmospheres, and is greater than 0.5 for low-O_2 Archaean-like atmospheres, which exceeds the stoichiometric limit that life can extract from CO_2 and H_2O substrates. Model-computed imbalances in CO and H_2 fluxes into and out of the model (not shown) further complicate and occasionally mask potential non-physical behaviour in other species. A more intuitive approach is to simulate volcanism and biology as 'fluxes' to which the composition of the atmosphere adjusts, which motivates our use of fixed flux LBCs.

4. Results from flux-driven photochemical modelling

We start with a 'flux-driven modern model,' which we construct as the best-fit model reproducing modern conditions using fixed flux LBCs for O_2, along with our 'Case 0' fixed flux LBCs for CH_4, H_2, CO and N_2O (Table 1). The model-predicted O_2 flux is 8.9×10^{11} pu, resulting in a CH_4:O_2 flux ratio of 0.094. While the modern gross O_2 production is much larger (∼4×10^{13} pu), our O_2 flux ignores very short-term sources and sinks of atmospheric O_2, while capturing the seasonal imbalance between O_2 production and destruction as well as the most important components of the short/medium-term carbon cycle (Zahnle et al., 2006). Our methane flux (8.4×10^{10} pu) is similar to the estimated net modern methane flux to the atmosphere from natural sources, after a large proportion of the gross methane production flux has been oxidised in sediments (Schlesinger and Bernhardt, 2013, p. 434).

We produced suites of model atmospheres to explore a range of non-modern biologic flux conditions, primarily by changing the absolute O_2 flux and CH_4:O_2 flux ratio. We cover a parameter space designed to simulate a range of possible states of primary productivity, methane production, methanotrophy and sulphate reduction. Specifically, we varied the O_2 flux between ∼0.01 to ∼40 times that of the flux-driven modern model, which we conceptually identify with varying levels of primary productivity. We assigned the CH_4 flux at various flux ratios from 0.094 (the CH_4:O_2 flux ratio in the 'flux-driven modern model') to 0.5 (the stoichiometrically-balanced ratio). The former is representative of the modern Earth system, and the latter is a commonly-assumed simplification for the late-Archaean biosphere (Catling and Claire, 2005; Daines and Lenton, 2016). Intermediate CH_4:O_2 flux ratios might represent biospheres with increasing anaerobic oxidation of

Table 1

Lower boundary conditions for the models described in this study. Units of flux are in photochemical units (1 pu = 1 molecule $cm^{-2} s^{-1} \sim 2.7 \times 10^{-10}$ Tmol yr^{-1}). Abbreviations are as follows: LBCs: lower boundary conditions; DV: deposition velocity; MR: mixing ratio. For Case 4, (a), (b) and (c) indicate the model suites with 'modern low,' 'modern high' and 'Archaean high' reducing fluxes, respectively.

Model	O_2	CH_4	CH_4:O_2 flux ratio	H_2	CO	N_2O	CO_2	Solar zenith angle
Atmos with Kasting and Donahue (1980) LBCs	MR: Varying	Flux: 1.34×10^{11} pu	N/A	Flux: 0 pu	Flux: 0 pu	Flux: 4.71×10^8 pu	MR: 2.57×10^{-4}	45°
Atmos with Kasting et al. (1985) LBCs	MR: Varying	Flux: 1.13×10^{11} pu	N/A	DV: 7.72×10^{-4} $cm\,s^{-1}$	Flux: 2.35×10^{11} pu	Flux: 4.21×10^8 pu	MR: 3.4×10^{-4}	50°
Atmos with Segura et al. (2003) LBCs	MR: Varying	Flux: 1.13×10^{11} pu	N/A	Flux: -1.02×10^{10} pu	Flux: 2.35×10^{11} pu	Flux: 4.21×10^8 pu	MR: 3.55×10^{-4}	45°
Atmos with Zahnle et al. (2006) LBCs	MR: Varying	MR: 10^{-4}	N/A	Flux: 3×10^{10} pu	Flux: 3×10^9 pu	MR: 3.1×10^{-7}	MR: 0.01	50°
Case 0	MR: Varying (2.1×10^{-11} – 0.42)	Flux: 8.4×10^{10} pu	N/A	Flux: 1.22×10^8 pu	Flux: 2.65×10^{11} pu	Flux: 4.11×10^8 pu	MR: 2.8×10^{-4}	50°
Flux-driven modern model	Flux: 8.9×10^{11} pu	Flux: 8.4×10^{10} pu	0.094	Flux: 1.22×10^8 pu	Flux: 2.65×10^{11} pu	Flux: 4.11×10^8 pu	MR: 2.8×10^{-4}	50°
Case 1	Flux: Varying (3×10^{10} - 4×10^{13} pu)	Flux: Varying	Varying: 0.094, 0.3, 0.45, 0.49	Flux: 1.22×10^8 pu	Flux: 2.65×10^{11} pu	Flux: 4.11×10^8 pu	MR: 2.8×10^{-4}	50°
Case 2	Flux: Varying (10^{11}, 3×10^{11}, 5×10^{11}, 10^{12}, 5×10^{12} pu)	Flux: Varying	Varying (0.1-0.5)	Flux: 1.22×10^8 pu	Flux: 2.65×10^{11} pu	Flux: 4.11×10^8 pu	MR: 2.8×10^{-4}	50°
Case 3	Flux: Varying (6×10^{10} - 4×10^{13} pu), and DV (see Section 4.4)	Flux: Varying	0.094	Flux: 1.22×10^8 pu	Flux: 2.65×10^{11} pu	Flux: 4.11×10^8 pu	MR: 2.8×10^{-4}	50°
Case 4	Flux: Varying (10^9-10^{12} pu)	Flux: Varying	(a): 0.16 (b): 0.16 (c): 0.15	Flux: (a): 2×10^9 pu (b): 10^{10} pu (c): 3×10^{10} pu	Flux: (a): 2×10^8 pu (b): 10^9 pu (c): 3×10^9 pu	Flux: (a): 4.1×10^8 pu (b): 4.11×10^8 pu (c): 4.11×10^8 pu	MR: 2.8×10^{-4}	50°
Case 5	Flux: Varying (10^9 – 10^{12} pu)	Flux: Varying	0.094	Flux (3.4×10^9) and DV (2.5×10^{-4} $cm\,s^{-1}$)	Flux (2.65×10^{11}) and DV (1.2×10^{-4} $cm\,s^{-1}$)	Flux: 4.11×10^8 pu	MR: 2.8×10^{-4}	50°
Case 6	Flux: Varying (3×10^{10} – 4×10^{13} pu)	Flux: Varying	Varying (0.1-0.5)	MR: 5.3×10^{-7}	MR: 1.1×10^{-7}	MR: 3.1×10^{-7}	MR: 4×10^{-4}	45°

methane in sediments resulting from increasing sulphate concentrations (Catling et al., 2007; Daines and Lenton, 2016; Habicht et al., 2002).

4.1. Case 1: varying O_2 fluxes at fixed CH_4:O_2 ratios

For a first test case, we varied O_2 flux between 10^{10} pu and 4×10^{13} pu. We produced 5 suites of up to 372 model atmospheres with O_2 fluxes between these values, with corresponding CH_4 fluxes set to maintain CH_4:O_2 flux ratios of 0.094, 0.3, 0.45 and 0.49. The model results, summarised in Fig. 2, are strikingly different to those using fixed mixing ratio LBCs.

Model-predicted O_2 (Fig. 2a) and CH_4 (Fig. 2b) surface mixing ratios are shown with the O_2 flux as the independent variable. For CH_4:O_2 flux ratios of 0.094, 0.3 and 0.45, pO_2 remains low (less than 10^{-7}) until the O_2 flux reaches a critical value, at which point pO_2 jumps to a new value above 4×10^{-4} within a trivial flux range. Computed methane mixing ratios drop just before the jump in pO_2, supporting suggestions that a collapse of methane might be a prerequisite for the GOE (Claire et al., 2006; Warke et al., 2020; Zahnle et al., 2006). Ozone column densities exhibit similar

patterns to pO_2, with clusters of solutions at low and high column densities without intermediates (Fig. 2c).

When a CH_4:O_2 flux ratio of 0.5 was used (results not shown in Fig. 2), the greater total flux of reductants (including H_2, CO and N_2O) than oxidants into the atmosphere resulted in a pO_2 always less than the CH_4 mixing ratio. For the 0.49 CH_4:O_2 flux ratio suite (Fig. 2a-c), the O_2 flux was eventually increased sufficiently such that it exceeded the total reductant flux, despite co-increasing methane fluxes. For this suite, there are 'Archaean-like' solutions with O_2 concentrations up to 10^{-6} and one steady-state atmosphere with an O_2 mixing ratio of 4×10^{-5}, followed by a series of solutions with pO_2 exceeding 3×10^{-3} (1.5% PAL).

To summarise, our 1222 'Case 1' models predict that oxygen, methane and ozone levels exist in one of two states – trace-O_2/O_3 solutions, and high-O_2/O_3 solutions – separated by a 'gap' in which there is only one (very specific) solution for intermediate O_2 surface mixing ratios. To better understand, we explored the detailed altitude-dependent chemistry of models spanning these states.

4.1.1. Two stable states of atmospheric chemistry?

We present mixing ratio profiles (Fig. 2d) and ground-level UV fluxes (Fig. 2e). Panels (i)–(iv) in Fig. 2d show O_2, O_3 and CH_4 mix-
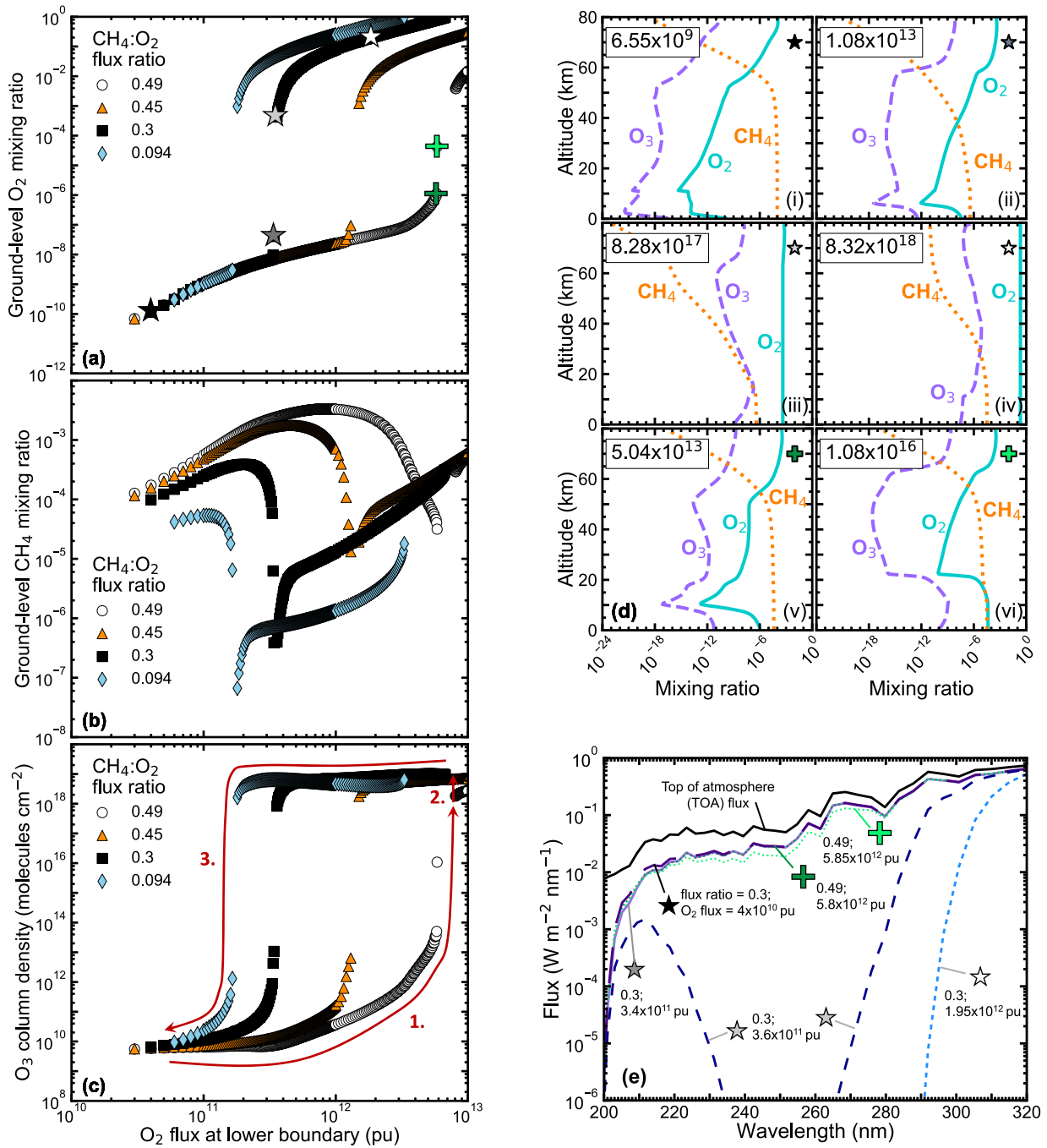
Fig. 2. Case 1 model results.
(**a**) Model-predicted ground-level O_2 mixing ratios with varying user-specified O_2 lower boundary flux, for different CH_4:O_2 flux ratios. Grey stars and green crosses indicate the O_2 lower boundary fluxes and mixing ratios of the six example model atmospheres examined in (d) and (e). Corresponding (**b**) model-predicted ground-level CH_4 mixing ratios, and (**c**) ozone column densities plotted against user-specified O_2 lower boundary flux. Red arrows on (c) illustrate the potential positive feedback discussed in Section 5. (**d**) O_2 (teal, solid lines), O_3 (purple, dashed lines) and CH_4 (orange, dotted lines) mixing ratio profiles for six example model solutions. Each panel refers to a model solution, indicated by a star or cross, on (a). Panels (i)–(ii) show two trace-O_2/trace-O_3 atmospheres with a CH_4:O_2 flux ratio of 0.3; panels (iii)–(iv) show two high-O_2/high-O_3 atmospheres, also with a CH_4:O_2 flux ratio of 0.3. Panels (v) and (vi) are for two atmospheres with a CH_4:O_2 flux ratio of 0.49. Ozone column densities are shown in the top left corners (units = molecules cm^{-2}). (**e**) UV ground flux with wavelength for the six example solutions shown on (a)/(d). The 'top of the atmosphere' (TOA) flux is also shown (black line). The labels for each model atmosphere refer first to the CH_4:O_2 flux ratio, and then to the O_2 flux across the lower boundary.

ing ratio profiles for four atmospheres with O_2 fluxes from the 0.3 CH_4:O_2 ratio suite, illustrating how vertical distributions change as O_2 and CH_4 fluxes increase. Panels (v) and (vi) show profiles of two atmospheres with CH_4:O_2 flux ratios of 0.49, isolating our only model atmosphere with ground-level pO_2 between 10^{-6} and 10^{-4}. The corresponding fluxes of UV photons that pass through the entire atmosphere and reach the surface are shown in Fig. 2e.

In the 'high-O_2/O_3' atmospheres (panels (iii) and (iv) in Fig. 2d), O_2 is well-mixed and more abundant than methane. In panel (iii), a modern-like stratospheric ozone layer is emerging, which is fully developed by panel (iv). The significant ozone shielding results in increased methane mixing ratios and low UV fluxes at the surface, with modern-like behaviour where no photons shortward of $\sim$290 nm reach the ground (Fig. 2e). The other high-O_2 atmosphere (panel (iii) in Fig. 2d) blocks substantial UV within the 200-320 nm

range, but some photons at DNA-damaging wavelengths (200-220 nm) will reach the ground. This case is similar to the Segura et al. (2003) (fixed mixing ratio boundary condition) model of 2.1×10^{-3} for O_2, which was argued to be the tipping point at which ozone shielding significantly impacts ground UV fluxes.

The panel (v) atmosphere is similar to those in panels (i) and (ii), while panel (vi) shows an atmosphere with tropospheric O_2 and CH_4 mixing ratios both approximately 80 ppm – on the cusp of the reducing/oxic divide. However, there is not sufficient ozone to provide tropospheric UV shielding of O_2 (Fig. 2e). While being a steady-state solution, it seems unlikely that this kind of atmosphere would be stable against small perturbations to the oxygen flux. The dearth of stable solutions between the trace-O_2 and high-O_2 attractors appears primarily due to positive feedbacks between increasing O_2 and O_3, which result in decreasing O_2 photolysis rates (Claire et al., 2006; Goldblatt et al., 2006). O_2 photolysis occurs only at wavelengths of 242 nm and below. The most abundant and effective absorbing molecule in the 200-300 nm wavelength range is O_3, with peak absorption at 240 nm. Increasing O_3 concentrations (Fig. 2c) therefore shield O_2 in the lower atmosphere from photolytic destruction (Figure A1), enabling O_2 concentrations to rise for a given flux. We explore this further in Section 4.3.

4.2. Case 2: varying CH_4:O_2 ratios at fixed O_2 fluxes

A second set of experiments designed to expand the parameter space of modelled fluxes investigates the reproducibility of our results under different conceptualisations of biogenic flux evolution. In the Case 2 suites, we fixed the absolute O_2 flux at five values (10^{11}, 3×10^{11}, 5×10^{11}, 10^{12} and 5×10^{12} pu), while decreasing the CH_4:O_2 flux ratio systematically from 0.5 to 0.1. These experiments might roughly capture the effects of increasingly sulphate-rich waters driving the locus of methane oxidation into sediments at a given primary productivity, but are admittedly a vast simplification of biospheric processes (Daines et al., 2017). The computed O_2 and CH_4 mixing ratios and corresponding O_3 column densities are shown in Fig. 3. As the CH_4:O_2 flux ratio is decreased from 0.5 to a critical value dependent on the absolute O_2 flux, an abrupt transition from reducing to oxidising atmospheres occurs (other than for an O_2 flux of 10^{11} pu, which is sufficiently low that this critical value is not reached for any CH_4:O_2 flux ratio less than 0.1). The Case 2 experiments demonstrate a wider 'gap' in solutions than Case 1, with no predicted model atmospheres with O_2 mixing ratios between 4×10^{-7} and 10^{-3}.

4.3. The photochemical (in)stability of atmospheres 'in the gap'

Atmospheres with O_2 mixing ratios between 4×10^{-7} and 4×10^{-4} are not produced in the flux-driven experiments described so far in this study, barring one case highlighted. By contrast, the identical numerical model utilising fixed mixing ratio boundary conditions produces results for all surface O_2 mixing ratios between 2.1×10^{-11} and 0.42 (Fig. 1). As all results in this and previous efforts are steady-state equilibrium solutions, it should be possible, numerically speaking, to carefully specify fixed flux boundary conditions to reproduce model atmospheres with any ground-level O_2 mixing ratio, even within the 'gaps' identified in Cases 1 and 2. To explore this, we chose three of our Case 0 fixed mixing ratio LBC models, with pO_2 values of 2.1×10^{-6}, 2.1×10^{-5} and 2.1×10^{-4}. We entered the predicted fluxes of O_2 (to 12 significant figures) as fixed flux boundary conditions and used the predicted species densities as initial values.

For each case, the flux-driven models did not converge when using the fluxes predicted by the fixed mixing ratio models. As fluxes were perturbed incrementally (at constant CH_4:O_2), no mod-
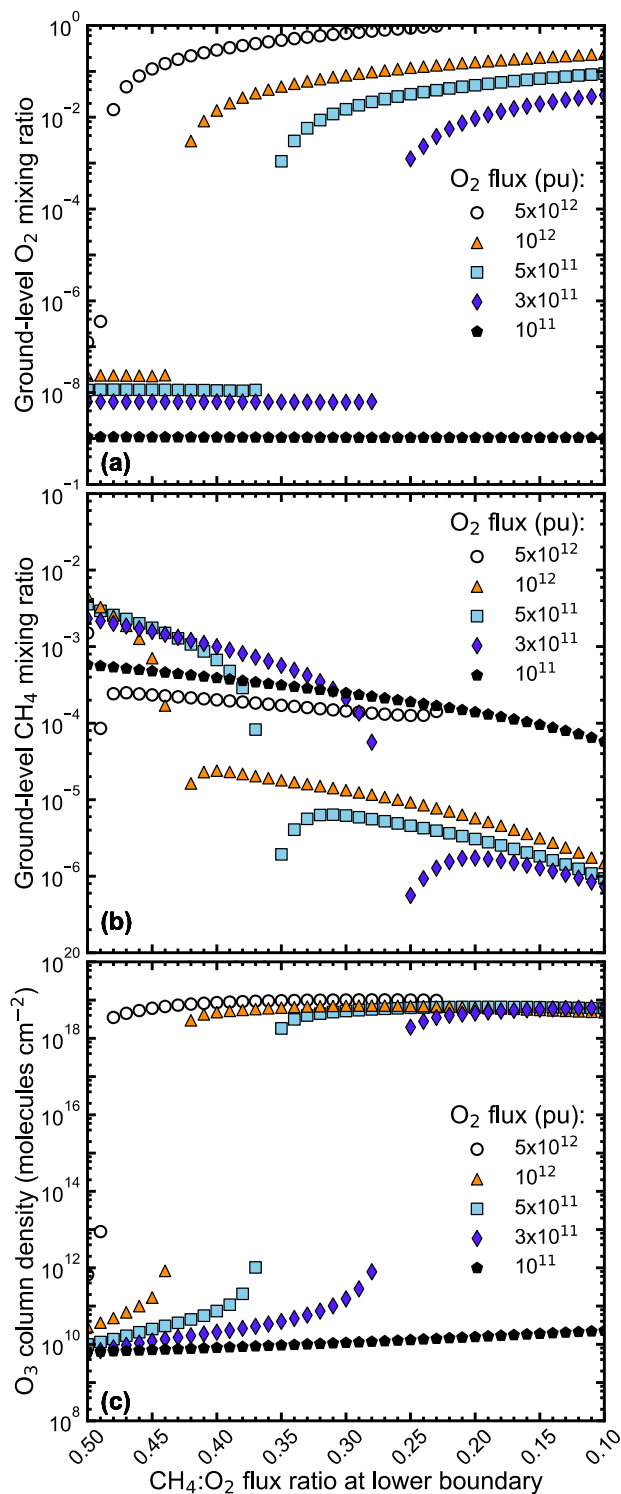
Fig. 3. Case 2 model results.
Model-predicted **(a)** O_2 ground-level mixing ratios, **(b)** CH_4 ground-level mixing ratios, and **(c)** O_3 column densities of model atmospheres, with decreasing CH_4:O_2 ratio. Five O_2 flux cases are shown, with the magnitude of the O_2 fluxes indicated by the legend, in photochemical units (1 pu = 1 molecule cm^{-2} s^{-1}).

els converged until the O_2 fluxes were $\sim$6%, $\sim$6% and $\sim$3% higher, or $\sim$1%, $\sim$1% and $\sim$4% lower than Case 0, respectively (Fig. 4). Subsequently, model solutions with $3 \times 10^{-8} < pO_2 < 5 \times 10^{-4}$ were not produced. Rounding our input fluxes to three significant figures for the 2.1×10^{-5} case to test for numerical precision issues made no significant difference to the results.
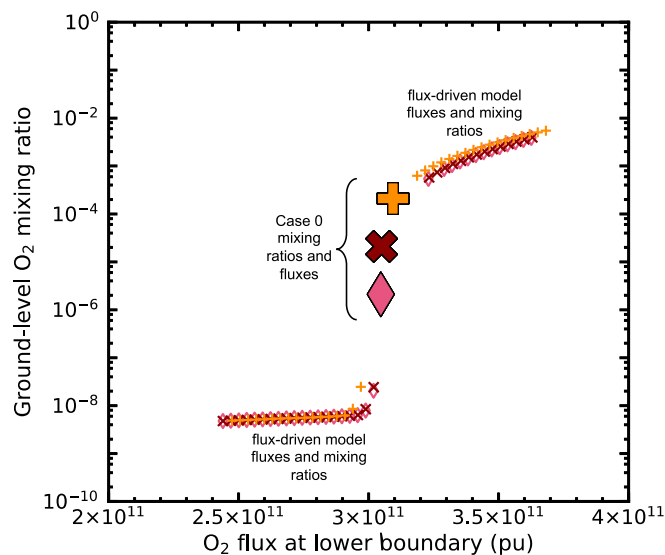
Fig. 4. Model-predicted ground-level O_2 mixing ratios of model atmospheres with fixed flux boundary conditions for O_2, where the user-specified flux is equal to predicted fluxes from the fixed mixing ratio-driven models (Case 0).

Large, filled yellow plus, red cross and pink diamond indicate the three chosen O_2 surface mixing ratios (2.1×10^{-4}, 2.1×10^{-5} and 2.1×10^{-6}, respectively), and the O_2 fluxes required by the fixed mixing ratio-driven model to produce these atmospheres. Small yellow plus, red cross and open pink diamond symbols indicate O_2 mixing ratios of atmospheres produced when fluxes for each case are perturbed slightly. Note that the x axis has a linear scale.

Fig. 5. Case 3 model results.
Model results showing the effects of the inclusion of an oxidative weathering flux of O_2 out of the atmosphere (Case 3 results; circles, triangles and squares) compared to the Case 1 model atmospheres, for which there is no drawdown O_2 flux (diamonds). Model-predicted ground-level O_2 (filled, teal symbols) and CH_4 (open, orange symbols) mixing ratios are plotted against user-specified O_2 flux into the model atmosphere across the lower boundary. The ratio of the CH_4 flux to the upward (into-the-atmosphere) O_2 flux is 0.094 for each model suite (Table 1). The equation for the drawdown flux is shown in the legend, where $[O_2]$ is the mixing ratio of O_2 and N_1 is the number density of the atmosphere in the lowermost grid step.

These tests supplement the preliminary conclusions from Cases 1 and 2, demonstrating that some steady-state model solutions computed using fixed O_2 mixing ratio LBCs between 4×10^{-7} and 5×10^{-4} are in fact unstable equilibrium solutions. They adjust to new solutions given trivial changes in lower boundary fluxes. This suggests, but does not fully prove, that fixed mixing ratio LBCs produce unstable equilibrium solutions in some (potentially large) regions of parameter space. A full stability analysis requires time-dependent computations beyond the scope of this effort, but will be forthcoming. Users of 1-D photochemical models (who must already carefully choose boundary conditions (e.g. Domagal-Goldman et al., 2014; Harman et al., 2018) are further cautioned to consider the stability of model results against small variations in flux, especially if using fixed mixing ratio boundary conditions.

4.4. Case 3: including negative feedbacks from oxidative weathering

Photochemical models to date have ignored a key negative feedback on oxygen fluxes at Earth's surface: as atmospheric O_2 concentrations build up, the removal rate via oxidative weathering increases. To test whether this could stabilise atmospheres with lower pO_2, we ran suites of models with the inclusion of deposition velocity boundary conditions that remove O_2 from the lower boundary at a rate proportional to the O_2 mixing ratio. Numerically, this requires the photosynthetic O_2 flux to be delivered into the atmosphere at 0.5 km above the surface, but this has a negligible effect on the vertical profiles because large eddy diffusion coefficients rapidly mix near-surface layers.

Firstly, we defined the O_2 lower boundary flux as $F_{out} = V_{dep}[O_2]N_1$, where V_{dep} is the deposition velocity (cm s^{-1}), N_1 is the atmospheric density in the first grid step, and $[O_2]$ is the ground-level O_2 mixing ratio. In a second suite, we used $F_{out} = V_{dep}[O_2]^{0.5}N_1$, following pyrite oxidation kinetics experiments that show a half-power law relation (Johnson et al., 2019). We focus on pyrite rather than organic carbon oxidation (which we consider a redox-neutral part of the reversal of photosynthesis in our conceptualisation), but conveniently carbon oxidation rate laws are also
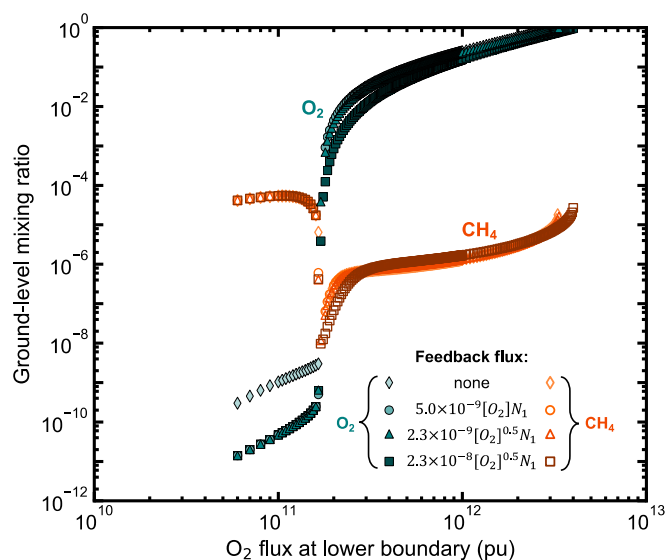
approximately half-power in O_2 (e.g. Daines et al., 2017). We tuned values of V_{dep} to 5×10^{-9} cm s^{-1} and 2.3×10^{-9} cm s^{-1}, respectively, in order to reproduce the modern oxidative weathering flux of $\sim 2.6 \times 10^{10}$ pu (Holland, 2002) and modern pO_2, when using the fixed-flux modern model. For a third suite, we increased V_{dep} by an order of magnitude for the half-power law case.

The results (Fig. 5) reveal that the two-state behaviour observed in Cases 1 and 2 persists in the Case 3 suites, despite the inclusion of a negative feedback flux. Increasing V_{dep} by an order of magnitude produces several steady-state model atmospheres with O_2 mixing ratios between 10^{-6} and 10^{-3}, but they are not stable against trivial changes in flux.

4.5. Confirmation of two stable states of atmospheric oxygen chemistry?

Fig. 6 illustrates a key result of this work. Predicted O_2 ground mixing ratios are plotted against O_3 column densities for the 2067 flux-driven steady-state model solutions in Cases 1-3. Given the monotonic increase in O_3 column density with O_2 mixing ratio for the classic (Case 0) result, it previously appeared plausible to imagine that Earth's atmosphere could have existed in a wide range of stable mid-oxic states. In contrast, our flux-driven results suggest that, for a broad range of O_2 and CH_4 fluxes, the majority of solutions cluster in two locations, with limited stable solutions between.

The model atmospheres show a bimodal distribution, with 'high-' (mode of 0.1-0.2) and 'trace-' (mode of 1-2 $\times 10^{-8}$) O_2 atmospheres (Fig. 6, upper panel). With 'high-O_2' atmospheres defined as those with pO_2 above 2.1×10^{-6} and, as a conservative measure, discarding the atmospheres with O_2 concentrations greater than 0.30 (since these are unlikely to have existed for most of the Phanerozoic), 95% (2σ) of our model atmospheres have pO_2 greater than 5×10^{-3}, and 97.5% have pO_2 greater than 2×10^{-3} ($\sim$1% PAL). The results may be additionally conservative as the bulk of the solutions computed with lower than 1% PAL O_2 were
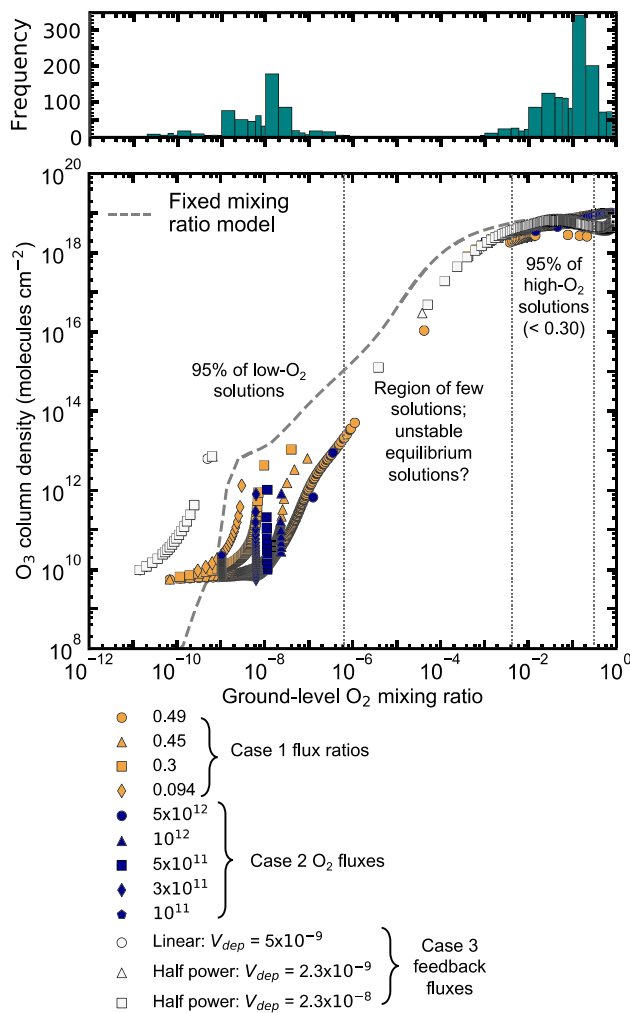
Fig. 6. Summary of Cases 1-3 compared to the classic model.
Upper panel: histogram showing frequency of model atmospheres with different ground-level O_2 mixing ratios (Cases 1, 2 & 3). Lower panel: O_3 column density plotted against O_2 mixing ratio for all model atmospheres in Cases 1 (orange symbols), 2 (purple symbols), and 3 (white symbols), compared to the results from the fixed mixing ratio-driven model (Case 0; grey dashed line). Vertical dotted lines indicate the regions of O_2 mixing ratio space in which most of the model solutions lie.

Fig. 7. Model-predicted ground-level O_2 mixing ratios plotted against K_{oxy}, for all model atmospheres from Cases 1-3.
Model atmospheres with $K_{oxy} < 1$ are reducing, while those with $K_{oxy} > 1$ are oxidising.

from cases in which oxidative weathering was set one order of magnitude higher than presently constrained values. With 'trace-O_2' atmospheres defined as those with pO_2 less than 2.1×10^{-3}, 95% of our model atmospheres have pO_2 less than 6×10^{-7}. While by no means a comprehensive statistical treatment, this supports previous studies (Claire et al., 2006; Daines and Lenton, 2016; Goldblatt et al., 2006; Laakso and Schrag, 2017), which concluded that there is a region of pO_2 parameter space spanning several orders of magnitude in which model atmospheric solutions are particularly sparse.

For Cases 1-3, the absolute fluxes of O_2 and CH_4 at which the atmospheres switch from reducing to oxic varies. Fig. 7 normalises this by plotting against K_{oxy}, which is defined as the O_2 source flux divided by the stoichiometrically-balanced average fluxes of all reducing gases (Catling and Claire, 2005). Model atmospheres with K_{oxy} less than 1 are reducing, and those with K_{oxy} greater than 1 are oxic, suggesting that the ratio of total reductant to oxidant flux determines in which of the two states the atmosphere lies. It further illustrates the very narrow range in flux space for which intermediate solutions beyond our 95% confidence bounds exist. If any of these lower pO_2 solutions were to persist in the

Earth system, they would require very strong (unspecified) negative feedbacks to maintain biologic fluxes in a tight window.

4.6. Exploring flux boundary conditions for other redox-relevant species

As a final set of tests, we examined the sensitivity of model output to the choice of boundary conditions for the reducing gases H_2 and CO. The H_2 flux has been shown to affect the pO_2 of steady-state model atmospheres (Laakso and Schrag, 2017). The two-state behaviour described above persists despite changes in the magnitude of reducing fluxes, and further strengthens our conclusion that the user-specification of boundary conditions must be carefully considered, even for trace species.

4.6.1. Case 4: magnitudes of reducing fluxes

For a fourth test case, we varied the magnitude of the fluxes of H_2, CO, H_2S and SO_2 into the model atmosphere, using the 'modern low,' 'modern high' and 'Archaean high' values from Zahnle et al. (2006; Table 1). When we used the 'modern low' fluxes as fixed flux LBCs for a model with fixed mixing ratio (modern-like) boundary conditions for O_2, CH_4 and N_2O, the resulting mixing ratios for H_2 and CO were 7.7×10^{-7} and 2.5×10^{-8}, which are slightly higher and lower than modern estimates, respectively (Ehhalt et al., 2001). Using the computed N_2O flux and fixed CH_4:O_2 flux ratio of 0.16, we produced a model suite with varying O_2 flux. We repeated this method for the 'modern high' and 'Archaean high' fluxes.

For all three scenarios, a jump from reducing to oxic atmospheric solutions within a narrow flux range was observed (Fig. 8). The 'gap' in O_2 mixing ratio solutions is slightly different to that produced in Cases 1-3, and again varies significantly over a range of O_2 fluxes. Regardless, the absolute magnitude of H_2 and CO fluxes (between end-member parametrisations) does not affect the overall two-state behaviour of the model atmospheres with varying user-specified O_2 flux.

4.6.2. Case 5: additional drawdown fluxes of reductants

Both H_2 and CO are consumed voraciously by microbes. We tested the model sensitivity to additional drawdown fluxes, by implementing a linear feedback flux equal to $V_{dep}[X]N_1$, where $[X]$ is the H_2 or CO mixing ratio. Following Zahnle et al. (2006), we chose deposition velocity values of 2.5×10^{-4} and 1.2×10^{-4} after Kharecha et al. (2005). We distributed the upward fluxes (from

Fig. 8. Cases 4 & 5 model results.
Model-predicted ground-level O_2 mixing ratios for model atmospheres, showing the effects of varying the fluxes of reducing species H_2, CO, H_2S and SO_2. Indigo squares, blue triangles and orange circles show the Case 4 results, for the 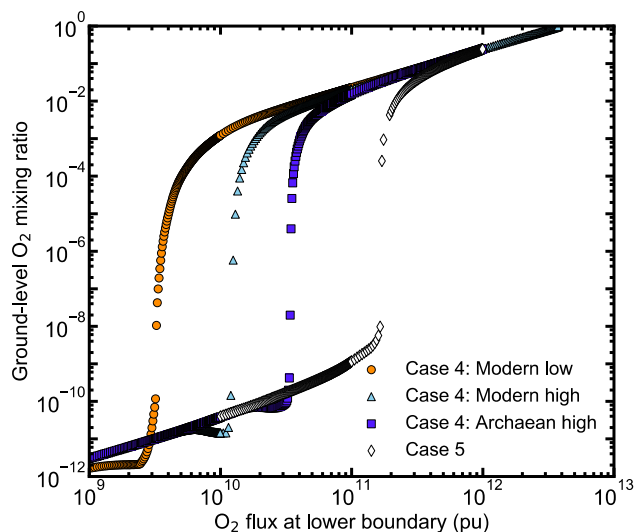'Archaean high,' 'modern high' and "modern low" magnitudes of fluxes from Zahnle et al. (2006), for H_2, CO, H_2S and SO_2, respectively. White diamonds show the Case 5 results, for which H_2 and CO are given additional deposition velocities (see Table 1).

the flux-driven modern model) log-normally through the first 10 km of the atmosphere (Zahnle et al., 2006). Using the mixing ratio of CO in the flux-driven modern model, we calculated the resulting downward flux and adjusted the upward flux such that the net flux remained the same as for Cases 1-3. Using the same method for H_2 resulted in a net downward flux, so we increased the upward flux until the net H_2 flux was positive (i.e. into the atmosphere). The resulting CO and H_2 mixing ratios were fairly similar to the global measured averages (6.2×10^{-8} and 5.5×10^{-7}, respectively; Ehhalt et al., 2001). Using these combined flux and deposition velocity conditions for H_2 and CO, we reproduced a suite of models with varying O_2 flux, at a constant $CH_4:O_2$ flux ratio (0.094). The results (Case 5 on Fig. 8) are our best attempt to properly model CO and H_2, and also display the two-state behaviour observed in Cases 1-3.

4.6.3. Case 6: mixing ratio boundary conditions for H_2 and CO – a cautionary tale

Using modern-like fixed mixing ratio LBCs for H_2, CO and N_2O produced results broadly similar to those described in previous subsections, in that there were reducing and oxic model atmospheres, and a transition between them within a very narrow flux range. However, this model setup (preliminary work presented by Gregory et al., 2019) also produced a third cluster of 'very-low O_2' atmospheres ($7 \times 10^{-7} < pO_2 < 3 \times 10^{-5}$; not shown), occurring only inside the narrow transition flux range, and featuring considerable ozone, but not a fully protective ozone shield. In addition, the 'high-O_2' atmospheres only had minimum O_2 mixing ratios of 10^{-2}, considerably affecting the application of our model to palaeo-O_2 levels over Earth history.

This demonstrates that the fixed mixing ratio LBCs of some trace gases enables the same numerical issues (potentially unphysical fluxes across the lower boundary) as for the more dominant species. Our results from Cases 1-5 with fixed flux boundary conditions for H_2 and CO allowed us to determine that the original three-state behaviour was driven by instabilities in the model-predicted lower boundary fluxes of H_2 and CO, which the model was switching between net input and output depending on the $CH_4:O_2$ flux ratio. This emphasises our primary conclusion that any photochemical modelling effort must fully describe choices for

boundary conditions, even for trace species, in order to allow reproducibility and assess reliability.

Having determined from Cases 4-6 that H_2 and CO flux boundary conditions produce rather different model atmospheres to mixing ratio LBCs, but that the magnitude of the fluxes and the inclusion of negative feedback fluxes do not affect the primary result of pO_2 bistability, we focus our discussion on Cases 1-3. While a full exploration of appropriate H_2 and CO lower boundary fluxes is beyond the scope of this paper, the 'flux-driven modern model' fluxes remain a good choice because of the better prediction of H_2 and CO ground-level mixing ratios, and their ease of comparison with previous 1-D photochemical modelling studies.

5. Discussion

5.1. Box models

Our results impact on previous work which predicts an abrupt shift from reducing to oxic atmospheres over an extremely narrow oxygen flux range (Alcott et al., 2019; Claire et al., 2006; Daines et al., 2017; Goldblatt et al., 2006; Laakso and Schrag, 2017). Despite extrapolating from the fixed-mixing ratio models we have called into question (e.g. Case 0), these box-model studies elucidated that flux-driven feedbacks within the Earth system drive a rapid transition between clusters of trace-O_2 and high-O_2 solutions, while passing through intermediates.

Model atmospheres with these 'intermediate' oxygen compositions have been produced by previous 1-D photochemical modelling efforts, but we have shown that some are unstable equilibrium solutions when explored in flux-driven photochemical models. Minuscule perturbations to lower boundary fluxes seemingly drive any intermediate 'solutions' towards attractors in high-O_2/O_3 or trace-O_2/O_3 regions of parameter space, due to positive feedbacks involving the formation of an optically thick ozone column (Claire et al., 2006; Goldblatt et al., 2006). While issues of kinetics remain to be determined, these atmospheric feedbacks will presumably occur much more rapidly than other biogeochemical feedbacks, which we predict would strongly amplify existing nonlinear behaviour in box models, as well as potentially drive strong feedbacks on microbial ecology. A full exploration of the dynamics of photochemical (in)stability and kinetic timescales for transitions requires time-dependent atmospheric models beyond the scope of this paper. Simultaneous incorporation of these short/medium-term atmospheric forcings into a long-term biogeochemical model with appropriate Earth system feedbacks would be an interesting target for future work.

5.2. Proterozoic pO_2

The lower limit of the high-O_2/O_3 solutions has interesting applications as a potential constraint on Proterozoic pO_2. Palaeo-O_2 levels over Earth history compatible with the regions of stability shown in this study are compared to proxy constraints in Fig. 9. Though our model results comment only on the potential stability of palaeo-O_2 levels, as opposed to their temporal evolution, we have truncated our regions of stability to fit with the commonly-accepted temporal constraints associated with the presence of S-MIF, O-MIF and charcoal. Our results are consistent with the estimates of Proterozoic pO_2 given by the absence of redox-sensitive minerals in Proterozoic sediments (e.g. Johnson et al., 2014), evidence for surface ocean oxygenation (Lenton and Daines, 2017), and the presence of variable $\delta^{53}Cr$ since 1390 Ma (Canfield et al., 2018). They are also consistent with (but stronger than) the lower limit of 2.1×10^{-4} indicated by the presence of an ozone layer (Segura et al., 2003), as revealed by non-zero O-MIF. However, since

Fig. 9. Summary of results from this study, in terms of palaeo-O_2 levels.

Purple regions show the ground-level O_2 mixing ratios of most of our model solutions in the context of existing constraints for pO_2 over Earth history. Grey regions show O_2 mixing ratios compatible with some proxies, from the review by Kump (2008). In addition, existing upper limit constraints are shown with downward arrows and annotations in italics (*Canfield, 1998, 2005; †Farquhar et al., 2000; Pavlov and Kasting, 2002; ‡‡Planavsky et al., 2014 (dashed line with circle end markers); ‡Cole et al., 2016; Planavsky et al., 2018 (dashed line with circle end markers)). Existing lower limits are shown with upward arrows and annotations in regular text (‡‡‡Canfield et al., 2018; Gilleaudeau et al., 2016 (dashed line with arrow end markers); ″Crockford et al., 2018; Segura et al., 2003 (dotted line); **Holland, 1994; Rye and Holland, 1998 (dotted line with diamond end markers)). Existing constraints from single points in time are shown by crosses (§Bellefroid et al., 2018; ¶Planavsky et al., 2020 (vertical line shows 90% confidence interval)). The post-Devonian charcoal record constraints are well-established, so we trim our constraints (purple regions) to fit with this.

this constraint arose from models using fixed mixing ratio boundary conditions, our results suggest a revision of the lower limit to 2×10^{-3}, as our flux-driven models produced very few solutions with both an ozone layer and pO_2 lower than this. Our results are inconsistent with arguments for low mid-Proterozoic pO_2 (e.g. Cole et al., 2016; Planavsky et al., 2014, 2020).

5.3. Earth system feedbacks and switches between states

Our results also prompt comments on the reversibility of the switch between the trace-O_2/O_3 and high-O_2/O_3 states. After an oxic atmosphere is established, is it possible to reduce biospheric fluxes, through a primary productivity crash or ecological reorganisation, to sufficiently low levels (with $K_{oxy} < 1$) such that the ozone layer collapses and pO_2 falls by several orders of magnitude? The continuous existence of terrestrial eukaryotic life precludes this scenario for most of the Phanerozoic, while the presence of O-MIF (Crockford et al., 2019) after the GOE strongly argues against a return to the trace-O_2/O_3 state during the bulk of the Proterozoic. Apparently, feedbacks between atmospheric chemistry of ozone formation and biospheric oxygen production are quite strong.

Our model results suggest a previously undescribed stabilising feedback to prevent such reversibility. We have assumed that $CH_4:O_2$ flux ratios of 0.5 and 0.1 are representative of reducing biospheres and the modern biogeosystem, respectively. With this in mind, consider a reducing atmosphere supported by a putative low productivity late Archaean biosphere featuring a low O_2 flux and a $CH_4:O_2$ flux ratio of 0.49. Following this suite of models (along the arrow labelled (1) in Fig. 2c), an increase in O_2 flux leads to a jump from the trace-O_2 to the oxic state, at an O_2 flux near 8.5×10^{12} pu in this example. In the resulting oxidising atmospheres, increased methane oxidation in sediments decreases the $CH_4:O_2$ ratio towards 0.1 (arrow labelled (2)). Subsequently, the decrease in O_2 flux necessary to plunge back into an anoxic world is far greater than for the higher $CH_4:O_2$ flux ratio values

(arrow labelled (3)). This constitutes a hysteresis loop preventing small decreases in O_2 flux from reversing atmospheric oxidation. The sulphate-dependent transition to lower $CH_4:O_2$ ratios is therefore a positive Earth-system feedback that helps maintain an oxic atmospheric state. In addition to time-dependent photochemical modelling, additional ecosystems modelling work is needed to consider this further, such as a study of the remineralisation dynamics and stability of sedimentary packages during the transition from Archaean-like $CH_4:O_2$ flux ratios of 0.5 to modern-like ratios below 0.1.

6. Conclusions

In this study we have shown that photochemical models utilising fixed flux boundary conditions can contribute towards constraints on atmospheric oxygen over Earth history. Even with the inclusion of long-term negative feedback fluxes of O_2, atmospheric chemistry drives the atmosphere towards one of two states, between which there are few stable equilibrium solutions. Our results specifically highlight a dearth of stable atmospheric configurations with pO_2 between 6×10^{-7} and 2×10^{-3}. Our results support estimates of trace-O_2 levels in the Archaean and O_2 levels greater than 1% PAL during the Proterozoic and Phanerozoic, and highlight the importance of carefully prescribed and described boundary conditions in photochemical models.

Declaration of competing interest

The authors declare that they have no known competing financial interests or personal relationships that could have appeared to influence the work reported in this paper.

by the European Research Council (ERC) under the European Union's Horizon 2020 Research and Innovation programme (grant no. 678812 awarded to M.W.C).

Appendix A. Supplementary material

Supplementary material related to this article can be found on-line at https://doi.org/10.1016/j.epsl.2021.116818.

References

Aiuppa, A., Shinohara, H., Tamburello, G., Giudice, G., Liuzzo, M., Moretti, R., 2011. Hydrogen in the gas plume of an open-vent volcano, Mount Etna, Italy. J. Geophys. Res., Solid Earth 116 (B10). https://doi.org/10.1029/2011JB008461.

Alcott, L.J., Mills, B.J., Poulton, S.W., 2019. Stepwise Earth oxygenation is an inherent property of global biogeochemical cycling. Science 366 (6471), 1333–1337. https://doi.org/10.1126/science.aax6459.

Arney, G., Domagal-Goldman, S.D., Meadows, V.S., Wolf, E.T., Schwieterman, E., Charnay, B., Claire, M., Hébrard, E., Trainer, M.G., 2016. The pale orange dot: the spectrum and habitability of hazy Archean Earth. Astrobiology 16 (11), 873–899. https://doi.org/10.1089/ast.2015.1422.

Bekker, A., Holland, H.D., Wang, P.L., Rumble III, D., Stein, H.J., Hannah, J.L., Coetzee, L.L., Beukes, N.J., 2004. Dating the rise of atmospheric oxygen. Nature 427 (6970), 117–120. https://doi.org/10.1038/nature02260.

Bellefroid, E.J., Hood, A.V.S., Hoffman, P.F., Thomas, M.D., Reinhard, C.T., Planavsky, N.J., 2018. Constraints on Paleoproterozoic atmospheric oxygen levels. Proc. Natl. Acad. Sci. 115 (32), 8104–8109. https://doi.org/10.1073/pnas.1806216115.

Bergman, N.M., Lenton, T.M., Watson, A.J., 2004. COPSE: a new model of biogeochemical cycling over Phanerozoic time. Am. J. Sci. 304 (5), 397–437. https://doi.org/10.2475/ajs.304.5.397.

Canfield, D.E., 1998. A new model for Proterozoic ocean chemistry. Nature 396 (6710), 450–453. https://doi.org/10.1038/24839.

Canfield, D.E., 2005. The early history of atmospheric oxygen: homage to Robert M. Garrels. Annu. Rev. Earth Planet. Sci. 33, 1–36. https://doi.org/10.1146/annurev.earth.33.092203.122711.

Canfield, D.E., Zhang, S., Frank, A.B., Wang, X., Wang, H., Su, J., Ye, Y., Frei, R., 2018. Highly fractionated chromium isotopes in Mesoproterozoic-aged shales and atmospheric oxygen. Nat. Commun. 9 (1), 1–11. https://doi.org/10.1038/s41467-018-05263-9.

Catling, D.C., Claire, M.W., 2005. How Earth's atmosphere evolved to an oxic state: a status report. Earth Planet. Sci. Lett. 237 (1–2), 1–20. https://doi.org/10.1016/j.epsl.2005.06.013.

Catling, D.C., Claire, M.W., Zahnle, K.J., 2007. Anaerobic methanotrophy and the rise of atmospheric oxygen. Philos. Trans. R. Soc. A, Math. Phys. Eng. Sci. 365 (1856), 1867–1888. https://doi.org/10.1098/rsta.2007.2047.

Claire, M.W., Catling, D.C., Zahnle, K.J., 2006. Biogeochemical modelling of the rise in atmospheric oxygen. Geobiology 4 (4), 239–269. https://doi.org/10.1111/j.1472-4669.2006.00084.x.

Cole, D.B., Reinhard, C.T., Wang, X., Gueguen, B., Halverson, G.P., Gibson, T., Hodgskiss, M.S., McKenzie, N.R., Lyons, T.W., Planavsky, N.J., 2016. A shale-hosted Cr isotope record of low atmospheric oxygen during the Proterozoic. Geology 44 (7), 555–558. https://doi.org/10.1130/G37787.1.

Crockford, P.W., Hayles, J.A., Bao, H., Planavsky, N.J., Bekker, A., Fralick, P.W., Halverson, G.P., Bui, T.H., Peng, Y., Wing, B.A., 2018. Triple oxygen isotope evidence for limited mid-Proterozoic primary productivity. Nature 559 (7715), 613–616. https://doi.org/10.1038/s41586-018-0349-y.

Crockford, P.W., Kunzmann, M., Bekker, A., Hayles, J., Bao, H., Halverson, G.P., Peng, Y., Bui, T.H., Cox, G.M., Gibson, T.M., Wörndle, S., 2019. Claypool continued: extending the isotopic record of sedimentary sulfate. Chem. Geol. https://doi.org/10.1016/j.chemgeo.2019.02.030.

Daines, S.J., Lenton, T.M., 2016. The effect of widespread early aerobic marine ecosystems on methane cycling and the Great Oxidation. Earth Planet. Sci. Lett. 434, 42–51. https://doi.org/10.1016/j.epsl.2015.11.021.

Daines, S.J., Mills, B.J., Lenton, T.M., 2017. Atmospheric oxygen regulation at low Proterozoic levels by incomplete oxidative weathering of sedimentary organic carbon. Nat. Commun. 8 (1), 1–11. https://doi.org/10.1038/ncomms14379.

Domagal-Goldman, S.D., Segura, A., Claire, M.W., Robinson, T.D., Meadows, V.S., 2014. Abiotic ozone and oxygen in atmospheres similar to prebiotic Earth. Astrophys. J. 792 (2), 90. https://doi.org/10.1088/0004-637X/792/2/90.

Ehhalt, D., Prather, M., Dentener, F., Derwent, R., Dlugokencky, E.J., Holland, E., Isaksen, I., Katima, J., Kirchhoff, V., Matson, P., Midgley, P., 2001. Atmospheric chemistry and greenhouse gases. No. PNNL-SA-39647. Pacific Northwest National Lab. (PNNL), Richland, WA (United States).

Farquhar, J., Bao, H., Thiemens, M., 2000. Atmospheric influence of Earth's earliest sulfur cycle. Science 289 (5480), 756–758. https://doi.org/10.1126/science.289.5480.756.

Farquhar, J., Zerkle, A.L., Bekker, A., 2014. Geologic and geochemical constraints on Earth's early atmosphere. In: Holland, H.D., Turekian, K.K. (Eds.), Treatise on Geochemistry: Reference Module in Earth Systems and Environmental Sciences, vol. 6: The Atmosphere – History, second edition. Elsevier, pp. 91–138.

Gilleaudeau, G.J., Frei, R., Kaufman, A.J., Kah, L.C., Azmy, K., Bartley, J.K., Chernyavskiy, P., Knoll, A.H., 2016. Oxygenation of the mid-Proterozoic atmosphere: clues from chromium isotopes in carbonates. Geochem. Perspect. Lett. 2 (2), 178–187. https://doi.org/10.7185/geochemlet.1618.

Glasspool, I.J., Scott, A.C., 2010. Phanerozoic concentrations of atmospheric oxygen reconstructed from sedimentary charcoal. Nat. Geosci. 3 (9), 627–630. https://doi.org/10.1038/ngeo923.

Glasspool, I.J., Scott, A.C., Waltham, D., Pronina, N.V., Shao, L., 2015. The impact of fire on the Late Paleozoic Earth system. Front. Plant Sci. 6, 756. https://doi.org/10.3389/fpls.2015.00756.

Goldblatt, C., Lenton, T.M., Watson, A.J., 2006. Bistability of atmospheric oxygen and the Great Oxidation. Nature 443 (7112), 683–686. https://doi.org/10.1038/nature05169.

Gregory, B.S., Claire, M.W., Rugheimer, S., 2019. Photochemical modelling of atmospheric oxygen levels reveals three stable states [abstract]. In: Goldschmidt Abstracts. 2019, p. 1201.

Habicht, K.S., Gade, M., Thamdrup, B., Berg, P., Canfield, D.E., 2002. Calibration of sulfate levels in the Archean ocean. Science 298 (5602), 2372–2374. https://doi.org/10.1126/science.1078265.

Harman, C.E., Felton, R., Hu, R., Domagal-Goldman, S.D., Segura, A., Tian, F., Kasting, J.F., 2018. Abiotic O₂ levels on planets around F, G, K, and M stars: effects of lightning-produced catalysts in eliminating oxygen false positives. Astrophys. J. 866 (1), 56. https://doi.org/10.3847/1538-4357/aadd9b.

Holland, H.D., 1994. Early Proterozoic atmospheric change. In: Bengtson, S. (Ed.), Early Life on Earth. Nobel Symposium. 1994, vol. 84. Columbia University Press, New York, NY, pp. 237–244.

Holland, H.D., 2002. Volcanic gases, black smokers, and the Great Oxidation Event. Geochim. Cosmochim. Acta 66 (21), 3811–3826. https://doi.org/10.1016/S0016-7037(02)00950-X.

Johnson, J.E., Gerpheide, A., Lamb, M.P., Fischer, W.W., 2014. O2 constraints from Paleoproterozoic detrital pyrite and uraninite. GSA Bull. 126 (5–6), 813–830. https://doi.org/10.1130/B30949.1.

Johnson, A.C., Romaniello, S.J., Reinhard, C.T., Gregory, D.D., Garcia-Robledo, E., Revsbech, N.P., Canfield, D.E., Lyons, T.W., Anbar, A.D., 2019. Experimental determination of pyrite and molybdenite oxidation kinetics at nanomolar oxygen concentrations. Geochim. Cosmochim. Acta 249, 160–172. https://doi.org/10.1016/j.gca.2019.01.022.

Kasting, J.F., Donahue, T.M., 1980. The evolution of atmospheric ozone. J. Geophys. Res., Oceans 85 (C6), 3255–3263. https://doi.org/10.1029/JC085iC06p03255.

Kasting, J.F., Holland, H.D., Pinto, J.P., 1985. Oxidant abundances in rainwater and the evolution of atmospheric oxygen. J. Geophys. Res., Atmos. 90 (D6), 10497–10510. https://doi.org/10.1029/JD090iD06p10497.

Kharecha, P., Kasting, J., Siefert, J., 2005. A coupled atmosphere–ecosystem model of the early Archean Earth. Geobiology 3 (2), 53–76. https://doi.org/10.1111/j.1472-4669.2005.00049.x.

Krause, A.J., Mills, B.J., Zhang, S., Planavsky, N.J., Lenton, T.M., Poulton, S.W., 2018. Stepwise oxygenation of the Paleozoic atmosphere. Nat. Commun. 9 (1), 1–10. https://doi.org/10.1038/s41467-018-06383-y.

Kump, L.R., 2008. The rise of atmospheric oxygen. Nature 451 (7176), 277–278. https://doi.org/10.1038/nature06587.

Laakso, T.A., Schrag, D.P., 2017. A theory of atmospheric oxygen. Geobiology 15 (3), 366–384. https://doi.org/10.1111/gbi.12230.

Lenton, T.M., Daines, S.J., 2017. Biogeochemical transformations in the history of the ocean. Annu. Rev. Mar. Sci. 9, 31–58. https://doi.org/10.1146/annurev-marine-010816-060521.

Lyons, T.W., Reinhard, C.T., Planavsky, N.J., 2014. The rise of oxygen in Earth's early ocean and atmosphere. Nature 506 (7488), 307–315. https://doi.org/10.1038/nature13068.

Pavlov, A.A., Kasting, J.F., 2002. Mass-independent fractionation of sulfur isotopes in Archean sediments: strong evidence for an anoxic Archean atmosphere. Astrobiology 2 (1), 27–41. https://doi.org/10.1089/153110702753621321.

Planavsky, N.J., Cole, D.B., Isson, T.T., Reinhard, C.T., Crockford, P.W., Sheldon, N.D., Lyons, T.W., 2018. A case for low atmospheric oxygen levels during Earth's middle history. Emerg. Top. Life Sci. 2 (2), 149–159. https://doi.org/10.1042/ETLS20170161.

Planavsky, N.J., Reinhard, C.T., Isson, T.T., Ozaki, K., Crockford, P.W., 2020. Large mass-independent oxygen isotope fractionations in mid-proterozoic sediments: evidence for a low-oxygen atmosphere? Astrobiology 20 (5), 628–636. https://doi.org/10.1089/ast.2019.2060.

Planavsky, N.J., Reinhard, C.T., Wang, X., Thomson, D., McGoldrick, P., Rainbird, R.H., Johnson, T., Fischer, W.W., Lyons, T.W., 2014. Low Mid-Proterozoic atmospheric oxygen levels and the delayed rise of animals. Science 346 (6209), 635–638. https://doi.org/10.1126/science.1258410.

Rye, R., Holland, H.D., 1998. Paleosols and the evolution of atmospheric oxygen: a critical review. Am. J. Sci. 298 (8), 621–672. https://doi.org/10.2475/ajs.298.8.621.

Schlesinger, W.H., Bernhardt, E.S., 2013. Biogeochemistry: An Analysis of Global Change, 3rd edition. Elsevier, Waltham, MA.

Segura, A., Krelove, K., Kasting, J.F., Sommerlatt, D., Meadows, V., Crisp, D., Cohen, M., Mlawer, E., 2003. Ozone concentrations and ultraviolet fluxes on Earth-like planets around other stars. Astrobiology 3 (4), 689–708. https://doi.org/10.1089/153110703322736024.

Warke, M.R., Di Rocco, T., Zerkle, A.L., Lepland, A., Prave, A.R., Martin, A.P., Ueno, Y., Condon, D.J., Claire, M.W., 2020. The Great Oxidation Event preceded a Paleo-proterozoic "snowball Earth". Proc. Natl. Acad. Sci. https://doi.org/10.1073/pnas.2003090117.

Zahnle, K., Claire, M., Catling, D., 2006. The loss of mass-independent fractionation in sulfur due to a Palaeoproterozoic collapse of atmospheric methane. Geobiology 4 (4), 271–283. https://doi.org/10.1111/j.1472-4669.2006.00085.x.